RSC Advances

PAPER

Cite this: *RSC Adv.*, 2016, **6**, 113240

Fluorine-tin oxide (FTO) electrode modified with platinum nanoparticles dispersed into montmorillonite clay as an effective and low cost catalyst for ethanol electrooxidation

Esmat Saghi,[a] Gholam Hossein Rounaghi,*[a] Ali Sarafraz-Yazdi,[a] Iman Razavipanah[a] and Parisa Mirhoseini Moosavi[b]

Received 27th July 2016
Accepted 14th November 2016

DOI: 10.1039/c6ra19087a

www.rsc.org/advances

This work demonstrates the use of montmorillonite (MMT) clay minerals as an effective and low cost catalyst support for Pt nanoparticles for electrocatalytic oxidation of ethanol molecules. Scanning electron microscopy (SEM), atomic force microscopy (AFM) and energy dispersive X-ray (EDX) spectroscopy were employed for the morphological study of the modified catalyst layers. The SEM images indicate that the platinum nanoparticles are dispersed in a homogeneous arrangement on a MMT matrix and the EDX spectrum confirms the presence of the Pt element. The results obtained from cyclic voltammetry measurements show that the FTO/MMT/Pt electrode is catalytically more active for electrooxidation of ethanol molecules than the FTO/Pt electrode. The electrochemical impedance spectroscopy (EIS) analysis and chronoamperometric measurements confirmed this result and the Tafel plots indicate better kinetics for ethanol electrooxidation in the presence of montmorillonite natural clays. The effect of some experimental factors such as the amount of MMT and Pt nanoparticles and the ethanol concentration were studied and the optimum conditions were obtained for electrooxidation of ethanol molecules using the FTO/MMT/Pt electrode.

1. Introduction

To meet the growing energy demand of the world, it is necessary to develop and implement medium and long term energy strategies based on a more environmentally friendly and sustainable model. Direct alcohol fuel cells (DAFCs), as clean energy conversion devices, have attracted a great deal of attention due to their high efficiency, high energy density and low or zero emissions.[1–4] Both direct methanol fuel cells (DMFCs) and direct ethanol fuel cells (DEFCs) have been projected to be strong candidates to compete with advanced batteries owing to their uniquely high specific energy. The toxicity of methanol, however, limits its wide spread use by consumers. By contrast, ethanol is a more attractive fuel for fuel cells due to providing an energy density very close to that of gasoline, nontoxicity, easy handling and storage unlike hydrogen fuel.[5–7] Furthermore, ethanol can be produced on a large scale from biomass.[8–10] Electrocatalytic oxidation of alcohols over various catalysts, which is based mainly on platinum, is the subject of interest of a great amount of researches. Pt is one of the best anodic materials that exhibits catalytic properties for the oxidation process of alcohols to proceed at a sufficient rate in fuel cells. But the high value of Pt is not cost effective for industrial applications. Consequently some research activities have been done to find new and less expensive materials as anodes for DAFCs. One of the ways to reduce the cost of fuel cell anodes, is deposition of platinum nanoparticles on the less expensive materials.[11–14]

Recently, developing the new supports for immobilizing the metal nanoparticles as electrocatalyst for fuel cells has become a subject of numerous researches.[15–17] Although organic polymers and polyelectrolytes have been more extensively studied as materials for coating electrode surface, but inorganic materials may also play an important role in this area because of their greater chemical and mechanical stability.[18]

According to Zhou article,[19] ion exchanged clay minerals can be designed and directly used as catalyst supports. Ion exchanged clay minerals and catalytic active component can interact with each other and then function through a synergistic effect. This partly explains that the dispersion of costly catalysts (*e.g.*, Pt, Au, Ru, Pd, and Rh) onto such a support material remarkably enhances the catalytic efficiency. Moreover, supported catalysts can minimize the cost of the production of commodity catalysts owing to the decrease of metal dosage, along with easy separation and then reuse.

[a]*Department of Chemistry, Faculty of Sciences, Ferdowsi University of Mashhad, Mashhad, Iran. E-mail: ghrounaghi@yahoo.com; ronaghi@um.ac.ir; Fax: +98 5138796416; Tel: +98 5137626388*

[b]*Department of Soil Science, Faculty of Agriculture, Ferdowsi University of Mashhad, Mashhad, Iran*

Previous studies have demonstrated that montmorillonite and related smectite clays can be used as coating to modify the electrochemical properties of the electrode surfaces substantially.[20]

The swelling phyllosilicate minerals are known as smectite clays.[21] The smectite clays share many of the desirable properties of cation exchange polymers for the modification of electrode surfaces.[20,22]

Montmorillonite is the most familiar and common member of the smectite group. The pore-like structure of MMT natural clay contains layers made up of two tetrahedral silica sheets fused to an edge-shared octahedral sheet of alumina.[21,23] Between these layers there are some monovalent and bivalent cations which can easily exchange with the other cations. Although MMT natural clays seems to be nonconductive but these monovalent and bivalent cations cause ionic conductivity. In the other word, MMT layers have cation exchange capacity which cause these layers to be conductive. MMT is abundant worldwide and does not require laborious and time-consuming efforts for their synthesis as well as surface functionalization. MMT has even more open framework structure than other porous materials and does not cause significant mass-transfer limitation. MMT is also chemical inert and environmentally friendly, which makes it a potential candidate as a promising support for fuel cell applications.[24]

The application of MMT as catalyst support has been reported previously. For example, MoO_3 catalyst which was supported on MMT, exhibited a higher activity in methanol oxidation.[24]

In the present research work, we studied the electrooxidation of ethanol molecules on a FTO electrode modified with MMT and Pt nanoparticles. FTO nanostructure was developed on the surface of a glass plate using spray pyrolysis method. Tin oxide impure with fluorine is an n type semiconductor. The band gap is larger than 3 eV (E_g = 3.6 eV). The FTO electrode was employed for construction of a novel and low cost electrocatalyst by using montmorillonite natural clay particles. The reason for our interest is that the silicate layers are very efficient adsorbents for organic molecules.[25] The electrocatalytic activity of FTO/MMT/Pt electrode toward the ethanol oxidation was investigated by means of different electrochemical methods such as cyclic voltammetry, chronoamperometry and electrochemical impedance spectroscopy (EIS). More discussion about these issues can be found in the next section. To the best of our knowledge, there are any reports about investigation of electrooxidation of ethanol molecules using FTO/MMT/Pt electrode.

2. Experimental

2.1. Material and reagents

All chemical reagents used in this experiment were of analytical grade. Perchloric acid, ethanol, stannous chloride, ammonium fluoride and $H_2PtCl_6 \cdot 6H_2O$ all purchased from Merck chemical company. They were used without any further purification. Montmorillonite was obtained from Fluka. All solutions were prepared with double distilled water.

2.2. Apparatus

The FTO nanostructure surface was developed by spray coating system (S.C.S. 92, Iran). The crystal structure of the FTO electrode was investigated using Philips PW1800 X-ray diffractometer (XRD) with Cu-K_α radiation (λ = 1.54 Å) and 0.04 degree step size. All of the electrochemical measurements except EIS analysis were carried out using a μ-Autolab type III electrochemical workstation with a conventional three electrode cell. The FTO electrode was used as working electrode and a platinum wire and an Ag/AgCl electrode (both from Azar electrode Co., Urmia, Iran) were used as counter and reference electrode, respectively. Electrochemical impedance spectroscopy studies were carried out using Gill AC potentiostat. The frequency range of 0.1 to 30 000 Hz and the modulation amplitude of 10 mV were employed for impedance studies. The surface morphological studies of FTO, FTO/Pt and FTO/MMT/Pt electrodes were investigated using scanning electron microscope (LEO1450VP) and atomic force microscope (Arapazhohesh, Tehran, Iran). Surface elemental analysis of the electrode was performed by energy dispersive X-ray technique using Oxford-7353 EDX microanalyzer.

2.3. Preparation of FTO electrode

FTO electrode was prepared by spray pyrolysis method. Glass plates were used as substrates. 33% stannous chloride, 3% ammonium fluoride, 32% ethanol and 32% doubly distilled water were mixed with each other under the stirring condition for 1 h. Then this solution was used by the spray coating system for preparation of FTO nanostructure surface. The carrier gas pressure for spray coating system was 3 atm. The normalized distance between the spray nozzle and the substrate was 40 cm. The spray rate was 5 mL min^{-1}. The substrate temperature was fixed at 500 °C. After formation the fluorine-tin oxide nanostructure on the surface of the glass plate, the FTO glass plate was cooled at room temperature for about 3 h. The glass plate with FTO nanostructure on its surface is referred as FTO electrode.

2.4. Preparation of FTO/MMT/Pt electrode

First of all, the FTO plate was cleaned sequentially for 10 min in a cleaner solution containing double distilled water and soap, 5 min in isopropanol, 5 min in ethanol and 2 min in acetone. Then as a typical process, 10.0 mg of MMT was ultrasonically mixed in 5 mL of water to form a homogeneous ink. 20 μL of this ink was dropped onto the surface of a FTO electrode (with a surface area of 25 cm^2) using a micropipette, and then dried with an IR lamp. Platinum nanoparticles were incorporated in the MMT film by electrochemical deposition from an aqueous solution of 2 mmol L^{-1} $H_2PtCl_6 \cdot 6H_2O$ and 0.2 mol L^{-1} perchloric acid using a potentiostatic technique. Potentiostatic loading of platinum was performed by keeping the potential of the electrode at −0.2 V.[26] The amount of Pt was evaluated from the quantity of electricity, Q_{dep}, used during the electrodeposition process at −0.2 V. Q_{dep} is calculated from the integral of I/t transient response. As the partial reduction of $PtCl_6^{2-}$ to Pt^{2+}

species should occur at potentials more positive than 0.11 V and the hydrogen evolution is negligible at −0.2 V,[27] a current efficiency close to 100% is expected.[28,29] Thus, the quantity of electricity, Q_{dep} (mC cm^{-2}), resulting from the $PtCl_6^{2-}$ total reduction is used for the evolution of deposited Pt. The Pt loading (W in mg cm^{-2}) is then:

$$W = Q_{dep}M/zF$$

where M is the atomic weight of Pt (195.078 g mol^{-1}), z is the number of the exchanged electrons (4) and F is the faradic constant (96 500 C per equivalent).

3. Results and discussion

3.1. Structural characterization

Fig. 1A, demonstrates the XRD pattern of FTO glass plate. As is clear in this figure, the diffraction pattern shows that the film has a tetragonal crystal structure with the cassiterite phase. The most intense diffraction peak is related to the crystal plane (200). The Debye–Scherrer formula was used for calculation the average crystal size:

$$D_{XRD} = K\lambda/\beta \cos\theta$$

where λ is the incident X-ray wavelength (1.54 Å), θ is the Bragg diffraction angle, β is the radian based full width at half maximum and K is the grin shape factor (0.94).[30] The FTO nanostructure grain size was 24.9 ± 0.2 nm based on using the above formula.

The SEM image of FTO's electrode surface is shown in Fig. 1B. As can be seen in this figure, a uniform and spongy surface is observed which lead to increase the surface area of the electrode. The EDX spectrum (Fig. 1C) indicates the presence of Sn, Si and O elements.

The SEM image of MMT natural clay is shown in Fig. 2A. As is evident in this figure, the MMT clay has a very rough surface with an irregular blocky morphology. The EDX spectrum of MMT (Fig. 2B) indicates the presence of Si, Al, O and Sn elements. The high intensity of Si peak is due to silicate layer of MMT which confirms that the MMT clay particles are dispersed onto the FTO electrode surface.

The morphology of the synthesized Pt nanoparticles as well as their dispersion on the MMT film can be evaluated from Fig. 2C. The inference that can be drawn from these micrograph is that the Pt nanoparticles are spread in a homogeneous arrangement on MMT film which indicates that the MMT natural clay acts as a good matrix for Pt nanoparticles deposition. Also the EDX spectrum (Fig. 2D) confirms the presence of the Pt element at the surface of the FTO/clay/Pt electrode. The schematic image of proposed electrodes is shown in Fig. 2E. As can be seen, Pt nanoparticles in the FTO/MMT/Pt is more available because the MMT natural clay provide three

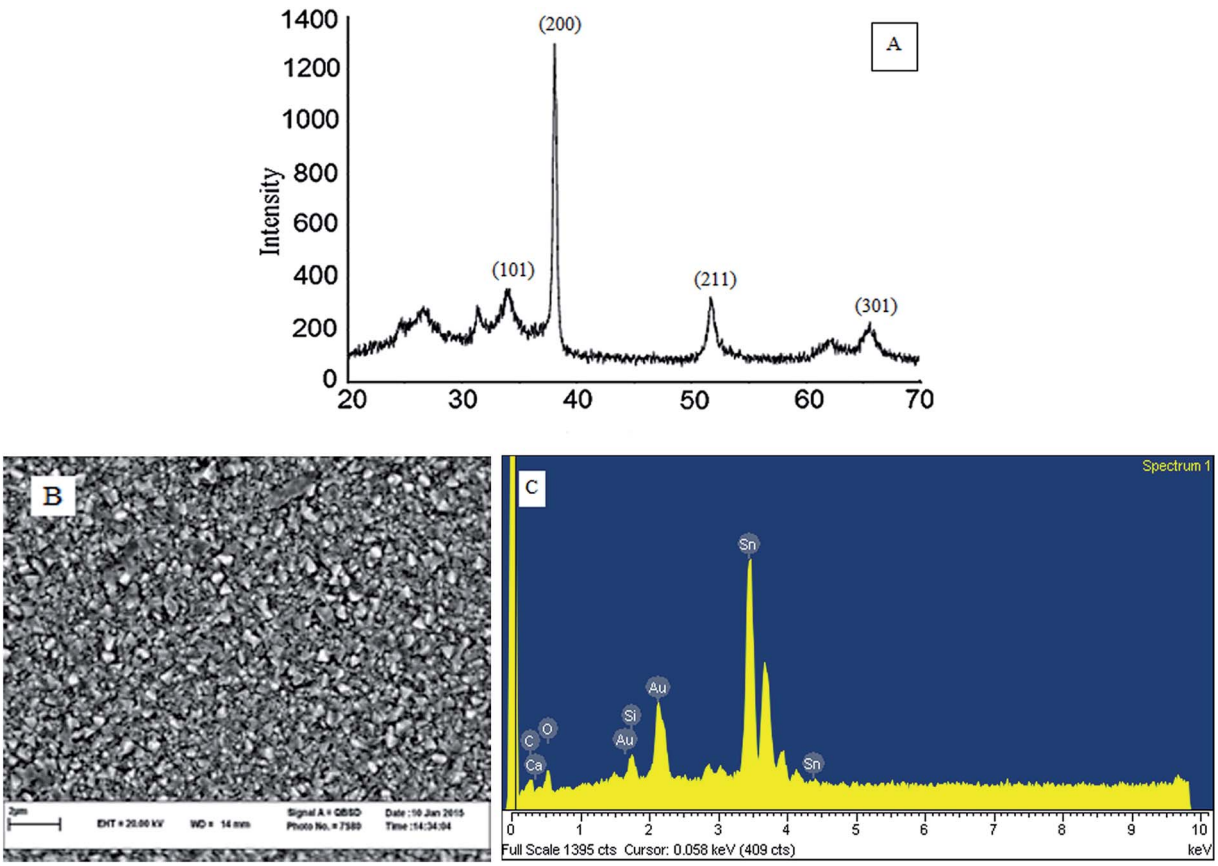

Fig. 1 (A) XRD pattern, (B) SEM image and (C) EDX spectrum of FTO glass plate.

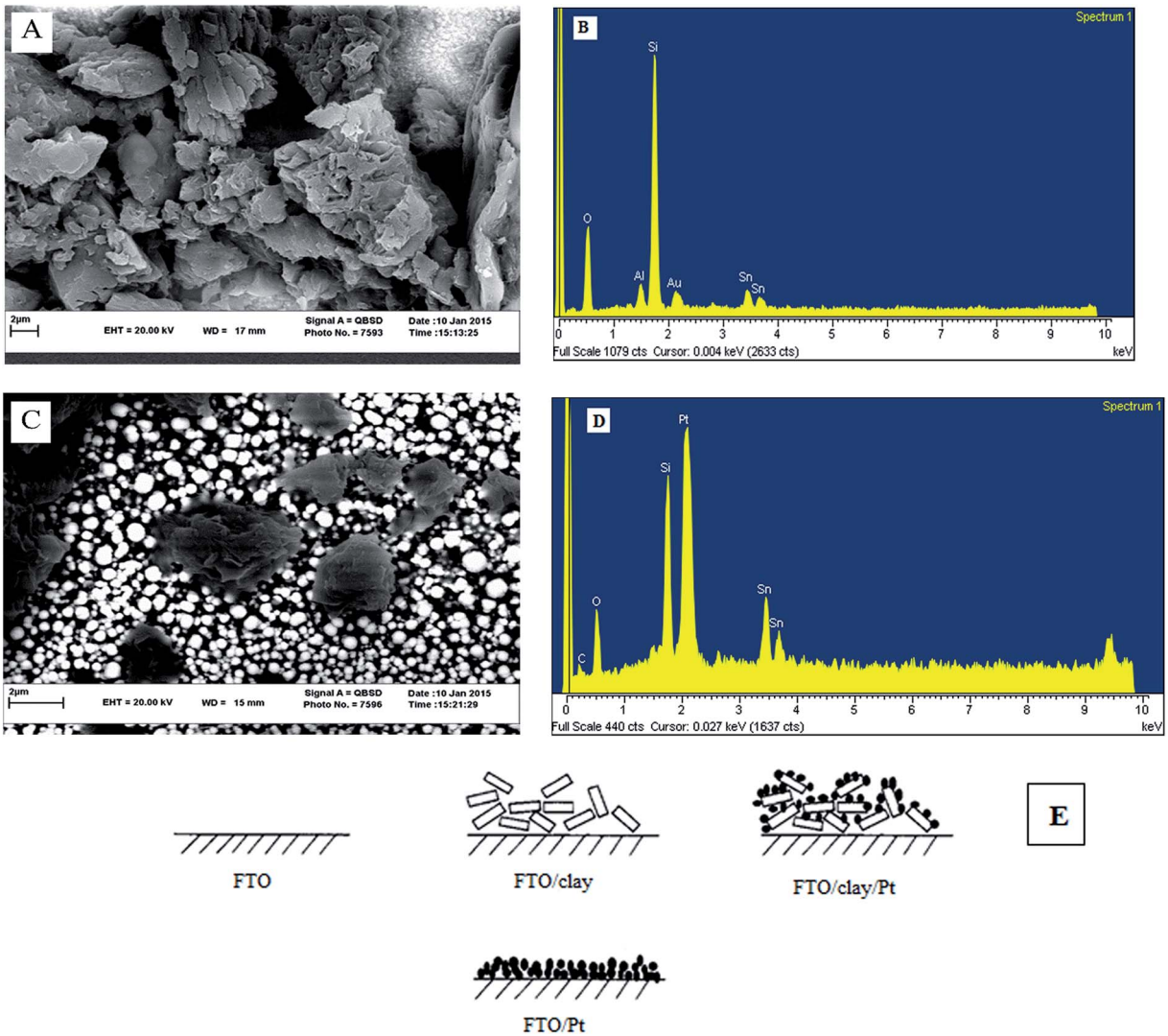

Fig. 2 (A) SEM image of MMT and (B) EDX spectrum of MMT, (C) SEM image of MMT/Pt, (D) EDX spectrum of MMT/Pt and (E) schematic of proposed microstructure of FTO, FTO/Pt, FTO/clay and FTO/clay/Pt electrodes.

dimensional matrix for Pt nanoparticles deposition, whereas in FTO/Pt electrode, the Pt nanoparticles are accumulating and cannot act very well.

3.2. Ethanol electrooxidation

The electrocatalytic activity of Pt nanoparticles confined in the MMT film was evaluated for oxidation of ethanol molecules and compared with FTO/Pt electrode. Fig. 3A, shows the cyclic voltammograms (CVs) of ethanol electrooxidation on FTO/MMT/Pt (Pt loading, 0.9 mg cm^{-2}) and FTO/Pt (Pt loading, 0.9 mg cm^{-2}) electrodes in 0.3 mol L^{-1} $HClO_4$ + 0.5 mol L^{-1} ethanol solution. All CVs are recorded by sweeping the potential from 0.0 to 1.5 V (*vs.* Ag/AgCl). As can be seen from this figure, two oxidation peaks at 0.88 V (a) and 1.32 V (b) are observed during positive potential scanning. In addition, in the reverse scan an anodic peak is detected at 0.46 V (c). Fujiwara and *et al.* used differential electrochemical mass spectrometry technique and they showed that the first oxidation peak (a) can be ascribed to CO_2 production and the second oxidation peak (b) appears due to formation of acetaldehyde.[31] Anodic peak in the reverse scan (c) corresponds to reoxidation of the ethanol molecules and intermediate species (*e.g.* Pt–OCH_2CH_3, Pt–$CHOH–CH_3$, $(Pt)_2COH–CH_3$, Pt–$COCH_3$ and Pt–CO) that are formed from incomplete oxidation of ethanol in forward scan stop.[32] These intermediates are oxidized hardly at low potentials and cause a catalyst poison.[33] A close inspection of Fig. 3A, clearly reveals that the FTO/MMT/Pt electrode has significantly a greater electrocatalytic activity than the FTO/Pt electrode. This finding can be attributed to the increase number of the catalytically active sites on the surface of FTO/MMT/Pt electrode for electrooxidation of ethanol molecules.

Fig. 3B depicts the cyclic voltammograms (CVs) of FTO/Pt and FTO/clay/Pt catalysts in 0.3 mol L^{-1} $HClO_4$ solution in the voltage range −0.35 to 1.3 V (*vs.* Ag/AgCl) at the scan rate of 50 mV s^{-1} at the room temperature. The electrochemical active surface area (ECSA) value is able to provide valuable

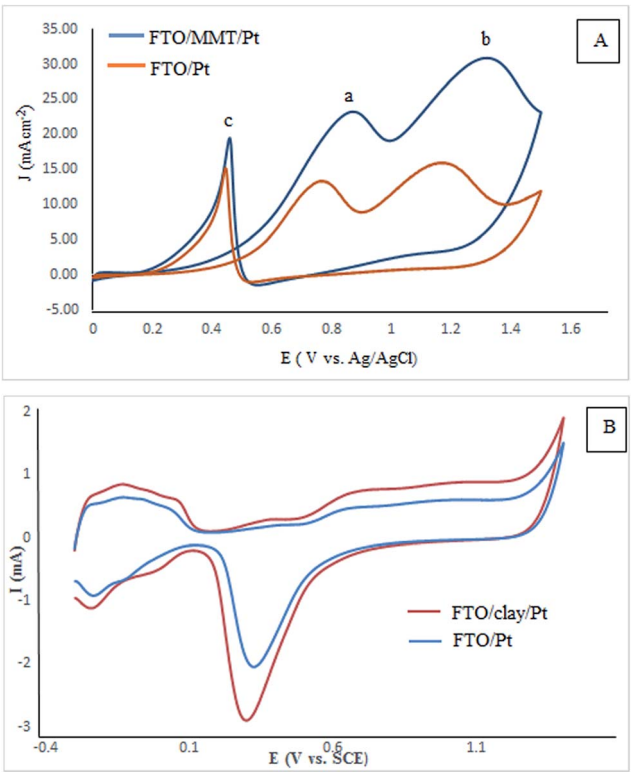

Fig. 3 (A) Cyclic voltammograms of electrooxidation of ethanol using FTO/Pt and FTO/MMT/Pt electrodes in 0.5 mol L^{-1} ethanol solution containing 0.3 mol L^{-1} $HClO_4$ at 50 mV s^{-1}, (B) Cyclic voltammograms of FTO/Pt and FTO/clay/Pt electrodes in 0.3 mol L^{-1} $HClO_4$ solution run at 50 mV s^{-1} at room temperature.

information about amount of electrochemically active sites on a mass basis of the precious metal and is also a crucial parameter for comparison of different electrocatalytic support. The ECSA of FTO/Pt and FTO/clay/Pt were calculated by following equation:[34]

$$\mathrm{ECSA} = Q_{\mathrm{H}}/[0.21 \times \mathrm{Pt}]$$

where Q_{H} (mC) is the charge exchanged during the electrodeposition of hydrogen on Pt at the potential range of −0.3 to 0.15 V (*vs.* Ag/AgCl), 0.21 is the charge (mC cm^{-2}) required to oxidize a monolayer of hydrogen on the Pt surface and Pt is the amount of Pt loading on the electrode surface. The ECSA of FTO/Pt and FTO/clay/Pt was found to be 1.16 and 1.48 cm^2 g_{Pt}^{-1} respectively. The ECSA of FTO/clay/Pt is 1.3 times higher than that of FTO/Pt, which is an evidence for formation of more electrochemically active sites on the surface of FTO/clay/Pt electrode.

3.3. Electrochemical impedance spectroscopy

In the electrochemical impedance spectroscopy measurement, Nyquist plot can be used to evaluate the electrochemical performance of a working electrode directly.[35] Fig. 4A, presents the Nyquist diagrams of FTO/Pt and FTO/MMT/Pt electrodes recorded at 1100 mV *vs.* Ag/AgCl electrode in the solution of 0.3 mol L^{-1} $HClO_4$ containing 0.5 mol L^{-1} ethanol. As is seen in this figure, the diagrams are half semicircle. The equivalent circuit compatible with the results of EIS studies presented in Fig. 4B. In this circuit, R_s, CPE, and R_{ct} represent solution resistance, a constant phase element corresponding to the double-layer capacitance, and the charge transfer resistance associated with the oxidation of ethanol, respectively.[36] The broadened semicircles with different diameters are described by parallel connection of R_{ct} and CPE.[37] The solution resistance can be found by reading the real axis value at the high frequency intercept. The real axis value at the other (low frequency) intercept is the sum of the polarization resistance and the solution resistance. The diameter of the semicircle is, therefore, equal to the polarization resistance so the lower value of R_{ct}, will result in a faster charge transfer reaction.[38] CPE can be obtained according to the equation represented below:[37]

$$\mathrm{CPE} = P^{1/n} R_{\mathrm{ct}}{}^{1-n/n}$$

In this equation, P is the pre-factor of the CPE, and n is its exponent that represents the deviation of the element from the ideal behavior. Table 1 shows the values of the equivalent circuit elements obtained by fitting the experimental results. As can be seen from Fig. 4A and the data in Table 1, the lower value of R_{ct} in the FTO/MMT/Pt electrode, suggests that the charge transfer process of ethanol oxidation occurring on the surface of FTO/MMT/Pt electrode is faster than FTO/Pt electrode. Thus the MMT/Pt nanocomposite offers a most conductive surface for oxidation of ethanol molecules in $HClO_4$ solution.

3.4. Effect of influencing parameters on electrooxidation of ethanol

3.4.1. Effect of MMT natural clay loading. As we pointed out, the MMT natural clay as a cheap and accessible material can increase the catalytic activity of the FTO/MMT/Pt electrode. In order to evaluate the optimum level of MMT natural clay for obtaining the maximum current density for ethanol oxidation, a series of experiments were carried out. Fig. 5A, shows the effect of the amount of MMT on the anodic peak current densities of ethanol oxidation. As is presented in this figure, the anodic peak current densities increase with increasing the amount of MMT natural clay up to 0.2 w/v% and drop afterwards. The increase in the peak current densities may be due to the better exfoliation of MMT up to 0.2 w/v% that provides three dimensional matrix for Pt nanoparticles deposition. On the other hand, the decrease in the peak current densities when the amount of MMT increases above 0.2 w/v%, can be correlated to the increase in the length of proton transfer pathways through the film in the presence of silicate layers.[39–41] Moreover, the increase in the amount of MMT above 0.2 w/v%, causes the formation of a compact and thick silicate layers which results in destroying the three dimensional matrix for Pt nanoparticles deposition. These phenomena result in decreasing the catalytic activity of the FTO/MMT/Pt electrode for ethanol oxidation. Therefore, for further studies, 0.2 w/v% was chosen as an optimum level of MMT natural clay. In order to investigate the textural changes of the clay, three point of the diagram was

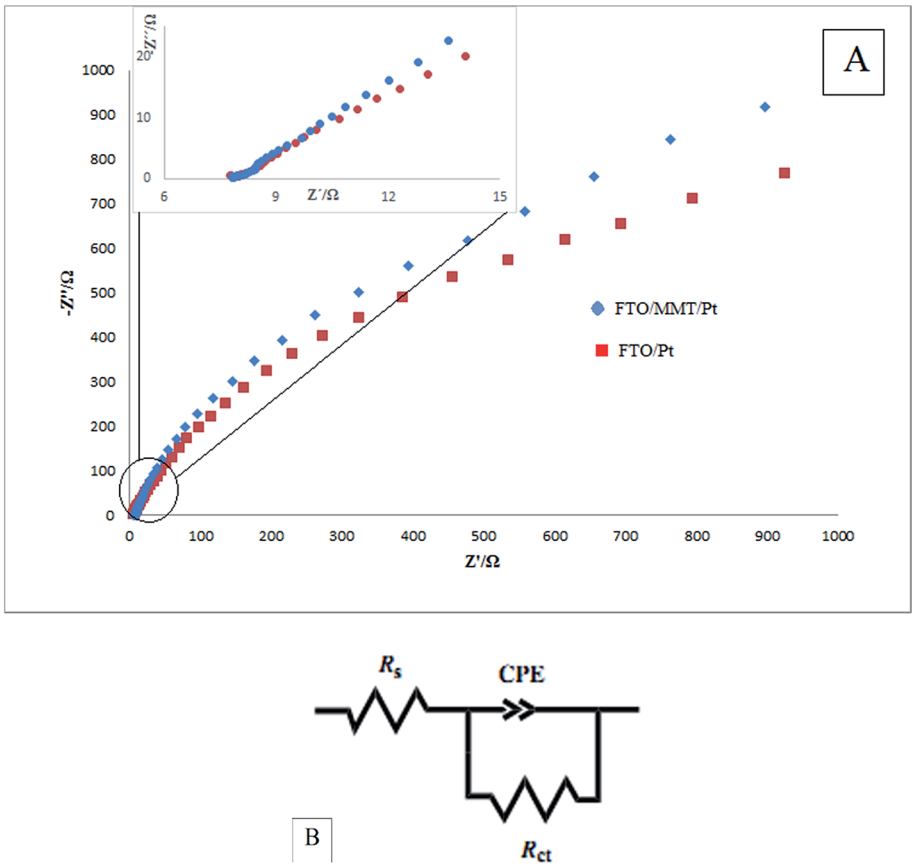

Fig. 4 (A) The Nyquist plots of FTO/Pt and FTO/MMT/Pt electrodes (inset: high frequency region of Nyquist plots), (B) equivalent circuit.

Table 1 The values of the elements in equivalent circuit fitted in the Nyquist plots of Fig. 4A

	R_{ct} (Ω cm^2)	P (μF cm^{-2})	n	CPE (μF cm^{-2})
FTO/Pt	2600	0.001	0.76	0.0011
FTO/MMT/Pt	2000	0.0009	0.86	0.0007

chosen and the AFM analysis was employed. Fig. 5B–D show the surface morphology of 0.04, 0.2 and 0.26 w/v% clay respectively. As can be seen, Fig. 5C is more roughness than two other points. These images clearly show that 0.2 w/v% level of MMT can provide better matrix for Pt nanoparticle deposition.

3.4.2. Effect of amount of Pt. The anodic peak current densities for ethanol oxidation at different Pt mass loading from 0.02 to 1.2 mg cm^{-2} over 0.2 w/v% MMT are shown in Fig. 6A. As is seen in this figure, the current densities increase with increasing the mass of Pt up to 0.9 mg cm^{-2} and then remain almost constant. This behavior may be due to the monotonously distribution of Pt nanoparticles on the silicate layers which gives rise to increasing the active surface area. However, any extra platinum loading over 0.9 mg cm^{-2} does not increase the catalytic activity of the electrode, probably because of the buried and inaccessible surface of Pt nanoparticles.[42]

3.4.3. Effect of ethanol concentration. Fig. 6B, shows the change of the oxidation current densities with the ethanol concentration. As is evident in this figure, the current densities increase with increasing the ethanol concentration up to 0.5 mol L^{-1} and then decrease. It seems that at higher concentrations of ethanol, the active sites at the surface of the electrode are saturated. Therefore, 0.5 mol L^{-1} ethanol concentration was considered as an optimum value.

3.5. Chronoamperometric studies

The chronoamperometric curves for oxidation of ethanol molecules were obtained using FTO/Pt and FTO/clay/Pt electrodes at the constant potential of 0.95 V (*vs.* Ag/AgCl) to determine the effect of the adsorbed intermediate products of ethanol oxidation such as CO at the surface of Pt nanoparticles. As is seen in Fig. 7, both electrodes present a continuous decay in activity with respect to time, which could be related to the remaining of the adsorbed intermediates such as CO at the surface of Pt nanoparticles. Inspection of Fig. 7 also shows that the current density in FTO/clay/Pt electrode decays more gently compared to the FTO/Pt electrode. Therefore, the FTO/clay/Pt is a better electrode than FTO/Pt for long time operation.

3.6. Tafel plots studies

Fig. 8, shows the Tafel plots for ethanol oxidation at FTO/clay/Pt and FTO/Pt electrodes. For further investigation of the effect

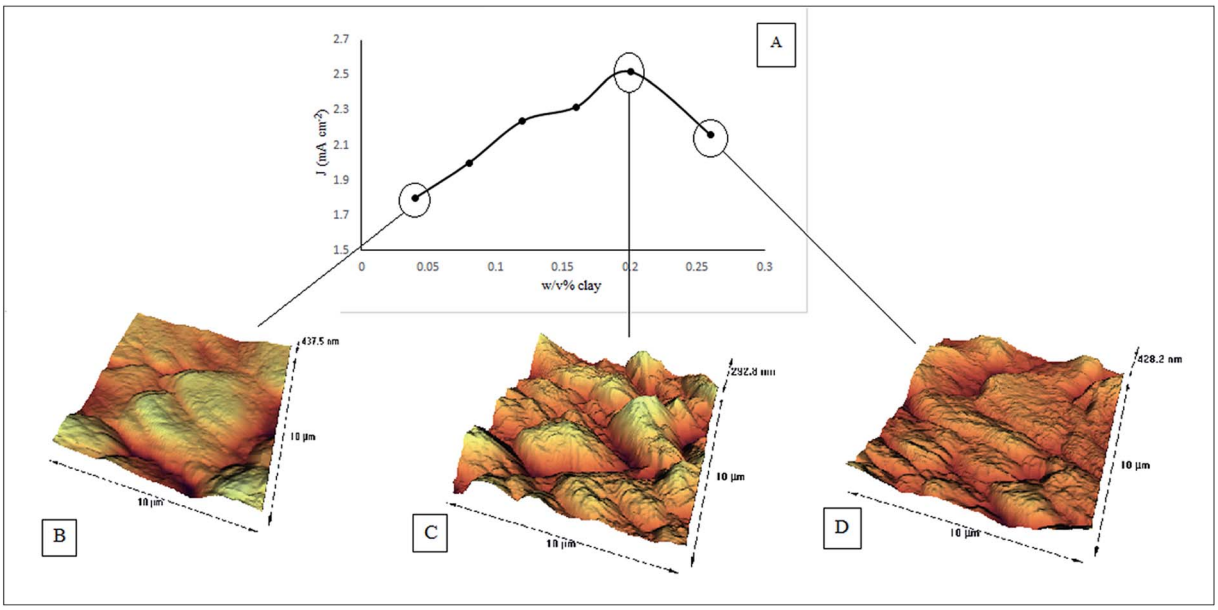

Fig. 5 (A) Anodic peak current of 0.5 mol L^{-1} ethanol in 0.3 mol L^{-1} $HClO_4$ as a function of various MMT loading, AFM image of (B) first point of diagram, (C) optimum level of clay and (D) final point of diagram.

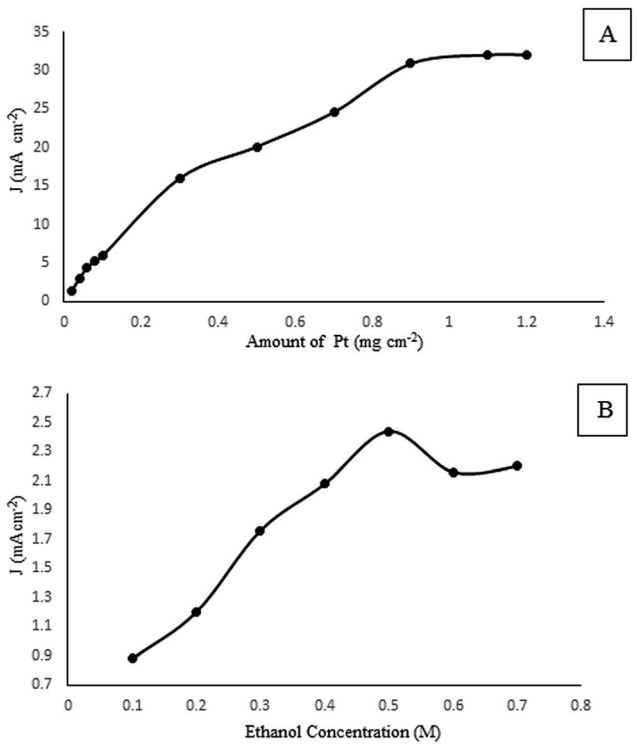

Fig. 6 Anodic peak current of (A) 0.5 mol L^{-1} ethanol in 0.3 mol L^{-1} $HClO_4$ solution as a function of platinum loading and (B) as a function of ethanol concentration at FTO/MMT/Pt electrode in 0.3 mol L^{-1} $HClO_4$.

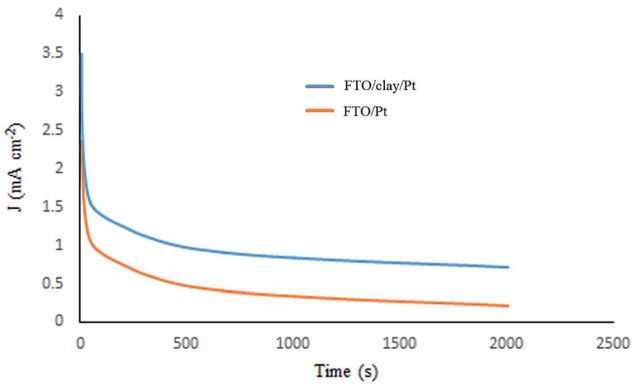

Fig. 7 Chronoamperometric curves of ethanol oxidation at FTO/clay/Pt and FTO/Pt electrodes, at a constant potential of 0.95 V *vs.* Ag/AgCl and at room temperature.

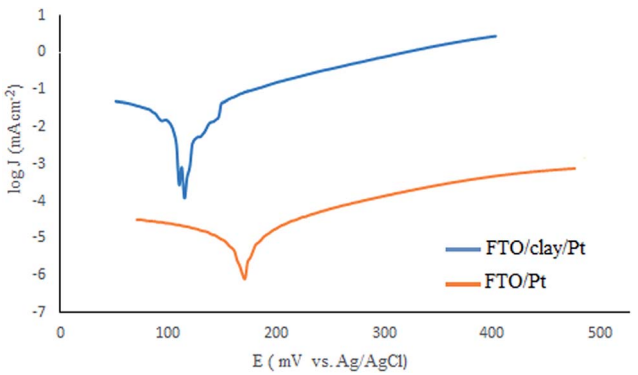

Fig. 8 Tafel plots of FTO/clay/Pt and FTO/Pt electrodes.

of montmorillonite layers on the electrocatalytic activity of Pt nanoparticle, the exchange current densities (J_0) of ethanol oxidation at these two modified electrodes were investigated. According to the Tafel equation,[43] the values of J_0 using the

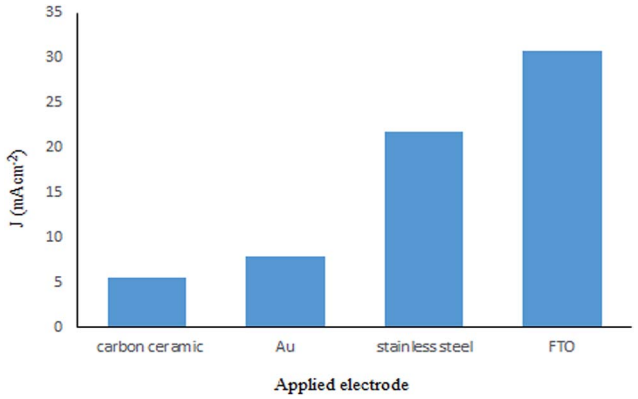

Fig. 9 Comparison of the anodic peak currents for ethanol electrooxidation at various electrode surfaces with the same amount of MMT and Pt loading in 0.5 mol L^{-1} solution of ethanol containing 0.3 mol L^{-1} $HClO_4$.

FTO/clay/Pt and FTO/Pt electrodes, were calculated and they were found to be: 1×10^{-2} and 2.5×10^{-6} mA cm^{-2}, respectively. The J_0 value in the case of FTO/clay/Pt electrode is about 4×10^3 times higher than that of the FTO/Pt electrode. This result suggests that the electrooxidation of ethanol molecules at FTO/clay/Pt electrode surface is easier from kinetic point of view because of the catalytic effect of the montmorillonite particles.

3.7. Catalytic efficiency of different electrodes

Fig. 9, illustrates the anodic current densities of ethanol electrooxidation at various electrode surfaces which were obtained by cyclic voltammetric method. Comparison of the graphical results which are shown in this figure, indicates that when the FTO surface is used for immobilization of montmorillonite clay and Pt nanoparticles, the higher anodic peak current densities is achieved compared to the Au, stainless steel and carbon ceramic surfaces. This behavior may be due to the nature of the FTO substrate which can enhance the surface area of the proposed electrode. Thus the FTO glass plate is the best surface for immobilization of the montmorillonite layers and Pt nanoparticles compared to the other electrode surfaces used in this study.

Table 2 Comparison between the current density (J_{pf}) and ratio of forward current to backward current (I_{pf}/I_{pb}) of FTO/MMT/Pt with some modified electrodes

No.	J_{pf} (mA cm^{-2})	I_{pf}/I_{pb}	Ref.
GCE/RGO/Pt	4.8	0.94	44
GCE/CuRGO/Pt	0.95	1.17	45
CCE/Pt	45	1.12	11
CPE/PtCuSn	1.15	1.92	46
CPE/PtCuRu	0.32	1.45	46
CPE/PtRuSn	0.2	2	46
FTO/MMT/Pt	30	1.5	This work

3.8. Comparison of electrocatalytic activity of FTO/MMT/Pt with some modified electrodes

For evaluation of the electrocatalytic activity of the prepared electrocatalyst, the electrocatalytic activity of the MMT/Pt was compared with some of the constructed modified electrodes. Table 2 summarizes some of the electrochemical characteristics of these electrodes such as peak current density (J_{pf}) and the ratio of forward current to backward current (I_{pf}/I_{pb}). As can be seen from the data in Table 2, the electrocatalytic activity of FTO/MMT/Pt electrode is better or comparable with the electrocatalytic activity of other modified electrodes.

4. Conclusion

In the present work, a modified fluorine-tin oxide (FTO) electrode was constructed for electrooxidation of ethanol molecules. The FTO glass plate was modified by montmorillonite (MMT) natural clay and platinum nanoparticles. The cyclic voltammograms, EIS analysis and chronoamperometric studies proved that the FTO/MMT/Pt electrode had much higher electrochemical activity toward the oxidation of ethanol molecules compared to FTO/Pt electrode. This effect can be attributed to the uniform dispersion of Pt nanoparticles in silicate layers of MMT natural clay. In addition, the Tafel plots showed that the electrooxidation of ethanol molecules at the FTO/MMT/Pt electrode is easier from kinetic point of view with respect to the FTO/Pt electrode. The results obtained in this study, reveal that the MMT natural clay can be considered as an ideal material for incorporation of Pt nanoparticles at the surface of the fluorine-tin oxide electrode for electrooxidation of ethanol molecules.

Acknowledgements

The financial supports of this research work from the Ferdowsi University of Mashhad-Iran (Grant No. 3/31326) are gratefully acknowledged.

References

1 S. T. Nguyen, H. M. Law, H. T. Nguyen, N. Kristian, S. Wang, S. H. Chan and X. Wang, *Appl. Catal., B*, 2009, **91**, 507–515.
2 H. B. Suffredini, G. R. Salazar-Banda and L. A. Avaca, *J. Power Sources*, 2007, **171**, 355–362.
3 L. Zhang, J. Zhang, D. P. Wilkinson and H. Wang, *J. Power Sources*, 2006, **156**, 171–182.
4 F. Vigier, S. Rousseau, C. Coutanceau, J. M. Leger and C. Lamy, *Top. Catal.*, 2006, **40**, 111–121.
5 F. Vigier, C. Coutanceau, F. Hahn, E. M. Belgsir and C. Lamy, *J. Electroanal. Chem.*, 2004, **563**, 81–89.
6 M. Z. F. Kamarudin, S. K. Kamarudin, M. S. Masdar and W. R. W. Daud, *Int. J. Hydrogen Energy*, 2013, **38**, 9438–9453.
7 Y. H. Chu and Y. G. Shul, *Int. J. Hydrogen Energy*, 2010, **35**, 11261–11270.
8 V. Comignani, J. M. Sieben, M. E. Brignate and M. M. E. Duarte, *J. Power Sources*, 2015, **278**, 119–127.

9 L. A. Rodríguez, M. E. Toro, F. Vazquez, M. L. Correa-Daneri, S. C. Gouiric and M. D. Vallejo, *Int. J. Hydrogen Energy*, 2010, **35**, 5914–5917.

10 E. C. Petrou and C. P. Pappis, *ACS Sustainable Chem. Eng.*, 2014, **2**, 2036–2041.

11 H. Razmi, B. Habibi and H. Heidari, *Electrochim. Acta*, 2008, **53**, 8178–8185.

12 B. C. H. Steele and A. Heinzel, *Nature*, 2001, **414**, 345–352.

13 C. K. Witham, W. Chun, T. I. Valdez and S. R. Narayanan, *Electrochem. Solid-State Lett.*, 2000, **3**, 497–500.

14 S. A. Kirillov, P. E. Tsiakaras and I. V. Romanova, *J. Mol. Struct.*, 2003, **651–653**, 365–370.

15 G. Fóti, C. Mousty, K. Novy, C. Comninellis and V. Reid, *J. Appl. Electrochem.*, 2000, **30**, 147–151.

16 M. H. Pournaghi-Azar and B. Habibi-A, *J. Electroanal. Chem.*, 2005, **580**, 23–34.

17 D. Stoychev, A. Papoutsis, A. Kelaidopoulou, G. Kokkinidis and A. Milchev, *Mater. Chem. Phys.*, 2001, **72**, 360–365.

18 H. Y. Liu and F. C. Anson, *J. Electroanal. Chem.*, 1985, **184**, 411–417.

19 C. H. Zhou, *Appl. Clay Sci.*, 2011, **53**, 87–96.

20 R. D. King, D. G. Nocera and T. J. Punnavia, *J. Electroanal. Chem.*, 1987, **236**, 43–53.

21 T. J. Pinnavaia, *Science*, 1983, **220**, 365–371.

22 D. Petridis, *Studies of clay modified electrodes, in multifunctional mesoporous inorganic solids*, Springer, Netherlands, 1993, pp. 433–450.

23 N. Sarier, E. Onder and S. Ersoy, *Colloids Surf., A*, 2010, **371**, 40–49.

24 D. Klissurski, D. Petridis, N. Abadzhieva and K. M. Hadjiivanov, *Appl. Clay Sci.*, 1996, **10**, 451–459.

25 J. Ménesi, L. Körösi, É. Bazsó, V. Zöllmer, A. Richardt and I. Dékány, *Chemosphere*, 2008, **70**, 538–542.

26 M. H. Pournaghi-Azar and B. Habibi, *J. Electroanal. Chem.*, 2007, **601**, 53–62.

27 K. Shimazu, D. Weisshaar and T. Kuwana, *J. Electroanal. Chem.*, 1987, **223**, 223–234.

28 H. Laborde, J. M. Leger and C. Lamy, *J. Appl. Electrochem.*, 1994, **24**, 219–226.

29 H. H. Zhou, S. Q. Jiao, J. H. Chen, W. Z. Wei and Y. F. Kunug, *J. Appl. Electrochem.*, 2004, **34**, 455–459.

30 S. Wu, A. Sun, F. Zhai, J. Wang, W. Xu, Q. Zhang and A. A. Volinsky, *Mater. Lett.*, 2011, **65**, 1882–1884.

31 N. Fujiwara, K. A. Friedrich and U. Stimming, *J. Electroanal. Chem.*, 1999, **472**, 120–125.

32 H. Wang, Z. Jusys and R. J. Behm, *J. Power Sources*, 2006, **154**, 351–359.

33 T. Iwasita and E. Pastor, *Electrochim. Acta*, 1994, **39**, 531–537.

34 R. Wang, T. Zhou, X. Qiu, H. Wang, Q. Wang, H. Feng, V. Linkov and S. Ji, *Int. J. Hydrogen Energy*, 2013, **38**, 10381–10388.

35 K. Ding, Y. Zhao, L. Liu, Y. Cao, Q. Wang, H. Gu, X. Yan and Z. Cuo, *Int. J. Hydrogen Energy*, 2014, **39**, 17622–17633.

36 J. B. Raoof, A. Nozad Golikand and M. Baghayeri, *J. Solid State Electrochem.*, 2010, **14**, 817–822.

37 M. R. Shoar Abouzari, F. Berkemeier, G. Schmitz and D. Wilmer, *Solid State Ionics*, 2009, **180**, 922–927.

38 G. Mousa, F. Golnaraghi, J. De Vaal and A. Young, *J. Power Sources*, 2014, **246**, 110–116.

39 M. Fallahi Samberan, M. M. Hasani-Sadrabadi, S. R. Ghaffarian and A. Alimadadi, *Int. J. Hydrogen Energy*, 2013, **38**, 14076–14084.

40 M. M. Hassani-Sadrabadi, N. M. Dorri, S. R. Ghaffarian, E. Dashtimoghadam, K. Sarikhani and F. S. Majedi, *J. Appl. Polym. Sci.*, 2010, **117**, 1227–1233.

41 M. M. Hassani-Sadrabadi, S. R. Ghaffarian, N. Mokarram-Dorri, E. Dashtimoghadam and F. S. Majedi, *Solid State Ionics*, 2009, **180**, 1497–1504.

42 B. Narayanamoorthy and S. Balaji, *Appl. Clay Sci.*, 2015, **104**, 66–73.

43 J. Wang, *Analytical Electrochemistry*, Wiley-VCH, New York, 2000.

44 F. Li, Y. Guo, T. Wu, Y. liu, W. Wang and J. Gao, *Electrochim. Acta*, 2013, **111**, 614–620.

45 F. Li, Y. Guo, M. Chen, H. Qiu, X. Sun, W. Wang, Y. Liu and J. Gao, *Int. J. Hydrogen Energy*, 2013, **38**, 14242–14249.

46 J. Barroso, A. R. Pierna, T. C. Blanco and N. Ruiz, *Int. J. Hydrogen Energy*, 2014, **39**, 3984–3990.